Numerical Studies on Turbulent Flame Propagation in Premixed Gas Deflagration inside a Tube

W.P. Fan and Y. Gao
College of Aerospace and Civil Engineering
Harbin Engineering University
Harbin, Heilongjiang, China

Y.M. Zhang
Hangzhou Steam Turbine & Power Group Co., Ltd
Hangzhou, Zhejiang, China

C.L. Chow
Department of Architecture and Civil Engineering
City University of Hong Kong
Hong Kong, China

W.K. Chow*
Research Centre for Fire Engineering
Department of Building Services Engineering
The Hong Kong Polytechnic University
Hong Kong, China

*Corresponding author:
Fax: (852) 2765 7198; Tel: (852) 2766 5843
Email: beelize@polyu.edu.hk; bewkchow@polyu.edu.hk
Postal address: Department of Building Services Engineering, The Hong Kong Polytechnic University, Hunghom, Kowloon, Hong Kong.

Funding

The work described in this paper was supported by a grant from the Research Grants Council of the Hong Kong Special Administrative Region, China for the project "A study on powder explosion hazards and control schemes when clouds of coloured powder are sprayed in partially confined areas" (Project No. PolyU 15252816) with account number B-Q53X.

March 2019

Numerical Studies on Turbulent Flame Propagation in Premixed Gas Deflagration inside a Tube

Abstract

Numerical simulation on turbulent flame propagation in premixed gas deflagration process in a tube will be reported in this paper, aiming at identifying the key factors affecting flame shape and flame velocity. Large eddy simulation with premixed gas combustion model is used to obtain results validated by full-scale experimental data. The effect of flow velocity and turbulence on flame propagation is discussed. The flow velocity of premixed gas is observed to be one of the main factors determining flame shape and affecting flame propagation process. The velocity difference of different parts of the flame front, both in magnitude and direction, will lead to tulip-shaped flame. Turbulence would accelerate the propagation of flame periodically. The cause of flame acceleration of low-intensity turbulence originates from two factors, namely, combustion and flow field, which transfer the heat and mass of chemical reaction from diffusion to vortex transport. As high-intensity turbulence will not affect the chemical reaction and the turbulent burning velocity, flame acceleration is controlled only by the characteristics of the flow field.

Keywords: large eddy simulation; deflagration; flame propagation; flow field characteristics

1. Introduction

Modelling the premixed gas flame propagation in tubes is important for studying explosion. Experimental observation of flame propagation is important in establishing associated theories. Accurately predicting the propagation characteristics of deflagration flame in tubes will lead to better understanding of dust explosion (Jenkins et al. 2013) and deflagration of the clean gas refrigerant (Chow 2014; Chow and Pang 2012; Ng and Chow 2015) in a confined space. Prevention and control of the explosion, safe storage and transportation of combustible gases and dust can be worked out accordingly based on the predictions in modelling. Physical experiments on premixed gas flame propagation in tubes would give the characteristics of flame propagation through high-speed photography and advanced measurement technology. However, experimental study is restricted by cost and scale. It is also difficult to analyze and predict the flame propagation of large-scale systems using experiments. Theoretical research is limited by the complexity and absence of information of many factors, such as chemical dynamics, turbulent combustion and flow, and the coupling effect among various factors. Thus, analytical model of flame propagation characteristics is not available. With the development of high-speed computers, numerical simulation with Computational Fluid Dynamics (CFD) for studying the deflagration of premixed gas in tubes becomes feasible. Current work in the literature mainly focuses on the application of numerical models and the study of the effect of some structural factors on the flame propagation phenomenon. There are few studies on the specific effects of flow on the basic characteristics of flame propagation. In this paper, numerical simulation of flame propagation in the premixed gas deflagration process based on the large eddy simulation (LES) method was carried out. The reliability of prediction was verified by experimental data. The effect of flow velocity and turbulence on flame shape and flame velocity in turbulent deflagration

process was elucidated.

Photographs on flame propagation for explosions in cylinders were provided by Ellis and Wheeler (1928). Flame shape in the front changed from convex to concave during propagation. The flame shape after this change was named as "tulip" flame (Salamandra et al. 1959). Characteristics of tulip flame were studied by Dunn-Rankin and Sawyer (1998). The process of premixed gas developing from weak ignition to tulip flame is basically controlled by the laminar burning rate and expansion ratio in laminar combustion. This process results from the propagation of inner laminar flame. Tulip flame is a special phenomenon in the development of flame propagation from laminar combustion to turbulent combustion in tubes. The study of its causes is valuable in explaining and predicting the change of flame shape.

In subsequent experimental researches, the effect of turbulence on flame propagation attracted more attention. Schlieren photography technology was used by Liberman et al. (2009) to study the accelerated propagation process of hydrogen-oxygen and ethylene-oxygen premixed gases, with deflagration to detonation transition (DDT) analyzed. Larger-scale experimental study by Thomas et al. (2010) focused on the premixed gas deflagration of methane, propane, acetone, acetylene and hydrogen with air. An empirical formula for calculating the velocity, pressure and DDT distance in a smooth and obstructed tube was proposed by Silvestrini et al. (2008). Effect of ignition source location on the DDT distance of hydrogen-air premixed gas in an 18-m long tube of diameter 0.15 m was reported by Blanchard et al. (2011). The height and density of obstacles in a long tube of square section were varied in the work of Teodorczyk et al. (2009) to study the deflagration process of hydrogen-air premixed gas. The results illustrated that obstacles would lead to momentum loss in flame propagation, and reduce the explosion power. However, the location and

blockage rate of obstacles would affect the DDT distance. Hydrogen-air and methane-air premixed gases under the conditions of different blocking ratios and obstacles were studied by Porowski and Teodorczyk (2013) in a 6-m long tube of diameter 0.14 m. A critical blocking ratio and the obstacle distance required for the acceleration of the premixed gas flame from deflagration to detonation were proposed. Orana and Gamezo (2017) proposed the critical conditions for deflagration detonation transition in obstructed channels. The effect of deflagration angle on pressure and other characteristics was analyzed by Rigby et al. (2015). The valuable data and results about the effects of turbulence on the transition of flame propagation state have been obtained in the above researches. In essence, this transition (deflagration to detonation) corresponds to the change of flame propagation velocity, and it is worth mentioning that further research on the mechanism of turbulence influence on flame velocity is still needed.

In numerical simulations, CFD model based on LES plays an important role. Irregular fold flame model instead of thin layer reaction zone model was used by Fureby (2005) to study the premixed combustion based on LES. This flame model yielded better predictions on the effect of flame stretching and bending on laminar combustion speed than other models. A kinetic model describing turbulent combustion velocity in LES was introduced by Knudsen and Pitsch (2008). The G equation model was combined with LES by Moureau et al. (2009) to simulate the preheating zone of turbulent flame. The effectiveness of different sub-grid models in LES for steady turbulent premixed combustion was compared by Di Sarli et al. (2010) through numerical simulation. Results showed that the sub-grid model proposed by Charlette et al. (2002) can predict the deceleration phenomenon when the flame accelerates and bypasses the obstacles. The predicted results are in agreement with the experimental data of flame speed and maximum pressure. A "Filtered Tabulated Chemistry for LES" was

proposed by Fiorina et al. (2010). LES was used by Gubba et al. (2011) to simulate the flow characteristics of the flame array through obstacles. Ng et al. (2017) and Huo and Chow (2017) carried out experimental and numerical studies on the propagation of liquefied petroleum gas deflagration in special spaces such as tube and garage, and studied the influencing factors of flame propagation velocity and deflagration overpressure. The factors affecting laminar flame propagation and turbulent flame propagation were studied respectively by Hermanns et al. (2010) and Ciccarelli and Dorofeev (2008). These works focused on the application and basic research of CFD numerical model in flame propagation, which is the premise of applying large eddy simulation (LES) model to actual flame propagation simulation and carrying out mechanistic research.

Premixed gas deflagration flame propagation process in a tube will be studied by CFD-LES in this paper using the software FLUENT. Flame propagation phenomenon will be validated by comparison with experimental data. By comparing the flame propagation distance, flame velocity and pressure from simulation and experiments, the reliability of the numerical simulation will be discussed quantitatively.

By combining CFD results with experimental observation, the mechanism of the deceleration and the formation of the “tulip” flame in flame propagation will be proposed and the acceleration mechanism of turbulence on flame propagation will be studied.

2. Computational Model

The physical process studied in this paper is on explosion of flammable gas and air mixed in a horizontal tube shown in Figure 1. The premixed gas is ignited at one end of the tube. The

flame forms around the ignition point and spreads around with shapes at different time $t_1 \ldots t_n$ shown. Initially, the flame front is in a smooth state of laminar combustion controlled by the laminar combustion velocity and expansion ratio, and its propagation speed increases with the increase of the area of the flame front. When the flame front touches the solid wall of the tube, the flame propagation velocity decreases with the decrease of the flame front area. The flame front changes from spherical shape to finger shape. Because of the different densities of unburnt premixed gas and combustion products on both sides of the flame front, the flame front has its own instability. Instability in propagation leads to wrinkling of the flame front, which increases the area of the flame front, causing the flame propagation speed to increase. The flame propagation further accelerates to the turbulent combustion stage. In a tube with no obstacle, turbulence is mainly caused by the wall effect and interaction between acoustic wave and flame front. Turbulence increases the burning rate by increasing the area of flame front and the rate of heat and mass transfer, and finally accelerates the propagation of flame front. In this process, the flame front is transformed from "finger" to "tulip" shape.

The flame propagation in the tube is a complex flow process coupled with chemical reaction. Assumptions are made to simplify the simulations as follows:

- The state parameters of premixed gas in the tube before ignition are 298K, 1.01325 x 10^5Pa.
- Premixed gas and combustion products are ideal gases.
- Combustion reaction is a one-step irreversible chemical reaction.
- The ignition source is an electric spark, and the ignition moment provides the premixed gas with enough energy to start the chemical reaction. The ignition process is very short. Thus the disturbance of the ignition source to the flow field can be ignored.

- Wall of the tube is adiabatic.
- The tube wall is rigid.

The differential equations for flow are given in Appendix A.

LES is a numerical simulation method lying between the direct numerical simulation (DNS) model and the Reynolds-averaged Navier-Stokes (RANS) model. The basic idea is to solve the motion of all turbulence scale vortices above a certain scale, so as to capture the large scale of many non-steady and non-equilibrium processes that the RANS method is incapable of. At the same time, it overcomes the huge computational cost of DNS due to the need to solve all turbulence scales.

Under low flame propagation speed (several ms^{-1}) much lower than the local sound speed, Navier-Stokes equations are set up through Fourier filtering, spatial filtering and Fourier average under low Mach number. The subgrid model is adopted to the solution of the equations. The Semi-Implicit Method for Pressure-Linked Equation (SIMPLE) in this model is used to calculate the pressure coupling equation.

The specific heat capacity, viscosity and thermal conductivity of premixed gas are calculated as follows:

$$\bar{c}_p = \sum_{i=1}^{n} c_{pi} y_i \tag{13}$$

$$\overline{\mu} = \frac{\sum_{i=1}^{n} \mu_i y_i M_i^{1/2}}{\sum_{i=1}^{n} y_i M_i^{1/2}} \tag{14}$$

$$\overline{\lambda} = \frac{\sum_{i=1}^{n} \lambda_i y_i M_i^{1/3}}{\sum_{i=1}^{n} y_i M_i^{1/3}} \tag{15}$$

In these formulas, c_p is the specific heat capacity at constant pressure, $\mathrm{J/(kg \cdot K)}$; μ is the coefficient of dynamic viscosity, $\mathrm{(N \cdot s)/m^2}$; λ is the coefficient of thermal conductivity, $\mathrm{W/(m \cdot K)}$; y_i is the molar concentration of the i^{th} component; and M_i is the molar mass of the i^{th} component, g/mol.

3. Numerical Simulations

The flame propagation experiment of methane-air premixed gas in a barrier-free square tube with different lengths reported (Dunn-Rankin and Sawyer 1998) in the literature was taken as an example in this paper. The FLUENT software was used to simulate this flame propagation process with two example cases, being Case 6 and Case 15 in Dunn-Rankin and Sawyer (1998). The basic information of the experiment (Dunn-Rankin and Sawyer 1998) is as follows:

- Methane-air premixed gas with equivalence ratio of 1.
- Experimental tube: the two ends of the tube are closed, the cross-section is 3.8 cm by 3.8 cm, the length is 6 cm in Case 6 or 15 cm in Case 15.

- Ignition source: Electric spark, located at one end of the tube with ignition energy of 30 mJ.

In the experiment, a Z-type Schlieren camera system was used to observe the flame propagation process (Dunn-Rankin and Sawyer 1998). The system is shown in Figure 2. The shooting frequency was 5000 frames/s with the pressure sensor set to measure the dynamic changes in the pressure in the tube with a sampling frequency 5000 Hz at the same time.

Based on the above experimental condition, numerical simulation was carried out for the three-dimensional unsteady state of the flame propagation process. The computational domain is shown in Figure 3, and the origin of the coordinate system is at the geometric center of the end face of the tube. The coordinates of the simulated regional boundary in the direction of *x*-*y*-*z* are *x*: 0 ~ 6 cm (or 15 cm), *y*: -1.9~1.9 cm, *z*: -1.9 ~1.9 cm.

The ignition source was at one end of the tube at coordinates x = 0.2 cm, y = 0 cm, z = 0 cm. The ignition source was set to the Spark Model with ignition started from 0 s to 0.001 s. The initial shape of the spark was a sphere with a diameter of 0.2 cm, which grew into a sphere with a diameter of 0.4 cm. The total energy of the ignition energy was 30 mJ.

Air is assumed to be composed of oxygen and nitrogen only. The chemical reaction between methane and air is:

$$CH_4 + 2\left(O_2 + 3.762N_2\right) \rightarrow CO_2 + 2H_2O + 7.524N_2 \quad (16)$$

The molar concentration (or volume fraction) of the combustible gas and air in the methane

air premixed gas with equivalent ratio of 1 is 9.50% to 90.50%, calculated according to the chemical reaction equation.

Other settings related to the simulation are shown in Table 1. The results of simulation are shown and discussed in the following section.

4. Flame Propagation Characteristics

The reported flame propagation process was captured (Dunn-Rankin and Sawyer 1998) through Schlieren photography with time intervals 2.5 ms in Case 6 and 5 ms in Case 15. As the camera was located at the tube side, the photograph corresponded to the *x*-*y* plane of the computing domain. *C* in the $z = 0$ plane of Case 6 and Case 15, representing the flame front, are shown in Figures 4 and 5. The flame propagation photographs and CFD simulated results at the same time are shown in those two figures with the tube coordinates matching with the experiments. The vertical axis is the *y* axis (-1.9 ~ 1.9 cm), the transverse axis is the *x* axis (the range of Case 6 is from 0 to 6 cm; Case 15, from 0 to 15 cm). In the numerical simulation, *C* represents the flame front. The flame surface morphology and flame propagation are represented by the mass fraction gradient of the combustion products. The range of *C* displayed is from 0.05 (blue colour) to 0.95 (red colour).

As shown in Figure 4, the flame spread from left to right with the flame front changed from semi-circle to "finger" in shape. From 2.5 ms to 7.5 ms, the propagation velocity of the flame front in the tube length direction (X axis) is faster than that in the tube radial direction (Y axis). The ratio of the propagation distance in the two directions (*x* and *y*) is close to 2 in the same time. After 12.5 ms, the flame front reaches the tube wall. The flame propagation

velocity near to the wall increases due to the boundary layer. The reverse flow caused by the reflected pressure wave from the closed end affects the flame front along the tube, which gradually becomes a flat surface. “Tulip” flame was not observed in the flame front due to the limitation of tube length (only 6 cm), which is consistent with the experimental results. The flame spreads only to the plane form at the end of the flame propagation. The flame propagation characteristics and the change of the flame front in the simulation are basically the same as the experimental results.

The results of simulation for Case 15 are shown in Figure 5. The flame propagation in Case 15 before 20 ms is basically the same as that in Case 6. At 25 ms, the bulge toward the ignition end appears on the flame front at the center of the tube (y = 0 m). The flame front then gradually develops into a “tulip” flame. The numerical simulation also predicts the change to "tulip" flame from 25 ms to 35 ms. This indicates that LES together with the premixed turbulent flame model and proper parameter selection can be used to simulate the flame propagation process.

5. Reliability of Numerical Simulation

The results of simulation are compared with the experimental results qualitatively in Figures 4 and 5 on the flame characteristics. However, reliability of the numerical simulation is not described quantitatively. Experimental results including flame propagation images and pressure data were provided (Dunn-Rankin and Sawyer 1998) in the literature. Through the treating of the flame propagation image, mean values of the flame propagation distance and flame velocity can be obtained. The reliability of numerical simulation can be determined by comparing the simulated results for the flame propagation distance, the average velocity of

flame and the pressure with experiments.

5.1 Flame propagation distance

Flame propagation distance is a key parameter to study flame propagation, and is also the basis for calculating flame velocity. The flame propagation distance can be obtained by judging the position of flame front according to the flame shape provided in the photographs in Dunn-Rankin and Sawyer (1998).

As the propagation velocity of flame along the axial direction for a horizontal tube is much larger than that in radial direction, the buoyancy effect is not significant when the propagation time is very short. The flame front is symmetrical about the center line of the tube. The experimental flame front position is plotted in the upper part and flame front position by simulation at the corresponding time is plotted in the lower part of Figures 6 and 7. The flame propagation distance is determined from flame front position, and the domain for comparison lies in the $z = 0$ plane, with y ranging from 0 to 1.9 cm in Figures 6 and 7. Based on a uniform scale grid, 6 and 4 points are selected for Case 6 and Case 15 respectively to represent the position of the flame front, and marked with ‘cross’ symbols in the figures.

Experimental and simulated results for the flame front positions under different axial positions are quantitatively compared in Figure 8. The closer the calculated value is to the experimental value, the closer the data points are to the line with slope = 1. The simulated results in Case 6 and Case 15 are very close to that of the corresponding experimental results. There are slight differences between them, and the data points are distributed on both sides of the line with slope = 1. For Case 6, the data points in the range of 0 ~ 4 cm are mostly

distributed below this line, indicating that the simulated values are smaller than the experimental values. The data points in the range of 4 ~ 5.5 cm are located above the line, indicating that the simulated values are larger than the experimental values. For Case 15, there are similar differences, but the corresponding range is different. In summary, the simulated values in the early stage of flame propagation are smaller, and becomes larger in the later stage. This indicates that the flame propagation velocity in the numerical simulation is slightly underestimated in the early stage.

5.2 Flame propagation speed

Photographs taken from the experiment in Dunn-Rankin and Sawyer (1998) were used to determine the position of flame front at different times. The mean flame velocity in the same time interval can thus be calculated. The experimental data of flame propagation speed determined is shown in Figure 9.

Propagation distance and average velocity of methane-air premixed gas flame at different times of Case 6 and Case 15 are shown in Figure 9(a) and (b). As buoyancy is negligible, the flame front shape is basically symmetrical about the central axis of the tube in the process of propagation. The upper part of the longitudinal section of the tube is selected for analysis. In the numerical simulation modeling, the central axis of the tube is taken to be along the x-axis. The range of the tube height is y from 0 cm to 1.9 cm. The propagation distance of the flame front and average velocity are calculated and analyzed on the horizontal line of y = 1 cm, avoiding the influence of the wall and the flow in the lower part of the tube. The flame propagation distance is determined by the transverse coordinates of the dots on the flame front in Figure 9. The longitudinal axis indicates the corresponding time of each photograph.

The ratio of the distance difference to the time between the adjacent intervals is the average of the flame velocity over this time interval.

Based on the following two criteria, the reliability of flame propagation velocity can be judged. On one hand, the variation of the simulated values should be consistent with the variation of the experimental flame velocity. As shown in Figure 10 (a) and (b), the circular points represent the average experimental values of the flame velocity, and the curve represents the simulated values. The reliability of the simulation could be verified by comparing flame acceleration and deceleration with the experimental results. On the other hand, the simulated average flame velocity should be comparable to the corresponding experimental values. It should be noted that experimental values only represent the average of flame velocity over a certain period or distance, with details neglected. In the numerical simulation, the instantaneous value of the flame velocity can be approached by the method of adjusting the time step, so that the neglected parts of the experiment can be deduced approximately. The average results of the instantaneous value, however, should be similar to the experimental values.

The variation in the experimental values of flame velocity in Figure 10 (a) and (b) show that the prophase of flame propagation is an acceleration process, and then gradually enters the deceleration stage along the tube in both cases. For Case 6, the range from 0 cm to 3 cm is the acceleration section, and the range from 3 cm to 5 cm is the deceleration section. Simulation yields the same variation of flame velocity as the experimental counterpart, with the range of acceleration and deceleration in agreement with experiment. For Case 15, the flame acceleration section is 0 ~ 3 cm and that for deceleration is 3 ~ 12 cm both by experiment and by simulation. Therefore, the numerical simulation results meet the first criterion for

reliability verification.

5.3 Pressure

The values of measured absolute pressure are given in the literature (Dunn-Rankin and Sawyer 1998). Because the experimental tube is short, the pressure waves propagate at the local sound speed, and the change of pressure is almost synchronous at any position of the tube. So the pressure at different sections is basically the same at the same time, and the choice of pressure monitoring location has little effect on the measurement results. In numerical simulation, a plane to monitor pressure change is set at regular intervals of 1 cm in the direction of the tube axis. Finally, the average of pressure values on all the monitoring surfaces at a certain time is used as the result of the internal pressure at this time. The comparison of pressure values by numerical simulation and experiment is shown in Figure 11.

Figure 11 (a) and (b) show the variation of pressure in the tube with time. The experimental data show that the pressure increases gradually with time, and there is a weak inflexion point in the process of pressure rising. This transition occurs near 15 ms and 20 ms respectively in Case 6 and Case 15, and the pressure increase rate decreases near these two time points. Compared with the previous analysis of the flame propagation process, it is found that these two moments are just the transition of the flame propagation from acceleration to deceleration, which reflects the influence of the change of flame velocity on pressure. Numerical simulation, however, does not reflect this change because of the arithmetical average operation on the data, which results in a smoothing effect around the moments of transition. Nevertheless, the simulated results are in accordance with experimental results,

both in value and in trend. Besides, the simulated value of pressure is smaller in the first half of the observation period and larger in the second half. It is mainly because in the experiment, the source of ignition will have some effect on the pressure inside the tube, but this factor is not considered in the simulation process, which causes the pressure simulation to be smaller than the experimental value. In the numerical simulation, the wall is assumed to be adiabatic but the actual tube wall is somehow thermally conductive. Thus the difference between the temperature caused by the adiabatic wall and the actual temperature gradually accumulates in the pressure calculation, which causes the later simulated pressure value to exceed the experimental value to a certain extent.

Through the analysis of the numerical simulation results of flame propagation of methane-air premixed gas in an obstacle-free tube, it is shown that the LES method and the premixed turbulent flame model can be used to simulate the flame propagation process under similar experimental conditions, and the simulated results have good reliability. At the same time, the computational resources can be saved substantially, and the simulated results can be used as the basis for further analysis.

6. Flow Field Characteristics

The effect of two main characteristics of the flow field, namely flow velocity and turbulence, on flame propagation is considered. Compared with Case 15, there is no "tulip" flame in Case 6, and the flame propagation characteristics are relatively simple. In numerical simulation, Case 6 can be used to verify the reliability of the simulation. In the analysis of the physical laws, the physical process in Case 6 and Case 15 is the same, and there is no need to consider them one by one. Therefore, this section only studies the complex situation of Case 15 (L =

15 cm).

6.1 Flow velocity

The influence of flow velocity on flame propagation is mainly reflected in two aspects: speed and direction. The left column of Figure 12 shows the results of simulation of the flow field generated by the flame propagation in Case 15 at different times, together with the flame front. Under the premise of neglecting buoyancy, it is considered that the results of experiment and numerical simulation are symmetrical about the central axis of the tube. Thus, the flow field in the upper half of the tube is representative of the flow in the tube. The corresponding numerical simulation domain is $x = 0 \sim 6$ cm; $y = 1 \sim 1.9$ cm; $z = 0$ cm. The arrow indicates the direction and magnitude of the velocity, and the specific velocity values are given in the graph on the right side of Figure 12.

Taking the positive direction of the *x*-axis as positive, according to the velocity vector diagram and the direction of flow, the change of flow field in the flame propagation process can be divided into two stages. In the first stage, from ignition to 15 ms, the gas flow and flame propagation in the tube move along the positive direction of the *x*-axis. Although the flame front always discharges the combustion product backward (negative direction of the *x*-axis), the velocity of the combustion product is in the negative direction relative to the flame front. As the velocity of the flame in the positive direction is larger, the resultant velocity of the combustion product is positive, and the flame goes through the accelerated propagation process. The flame front also undergoes a morphological change from spherical to finger-shaped at this stage.

In the second stage, from 15 ms to the end of flame propagation, the flame front is gradually approaching the closed end of the tube. The compression effect of the premixed gas between the flame front and the closed end is becoming more and more significant, so that the pressure gradually increases and the flow direction begins to change. The velocity of premixed gas in front of the flame front is still in the same direction as the flame propagation, but the velocity is getting smaller and smaller. The velocity of the combustion product behind the flame front is opposite to the flame propagation direction. During this stage, the flame experiences the process of velocity decay, and the flame front begins to change to a planar shape. In addition, numerical simulation shows that the thickness of the flame array increases in this stage, which is related to the negative direction of flow velocity. The negative direction movement of the flow field and the combustion product itself strengthen the reverse transport of the combustion products, which is reflected in the numerical simulation results that the mass fraction of the combustion product (process variable C) is expanded and the flame front is thickened.

The above analysis shows that the velocity direction of the flow field can affect the flame propagation, and the change of the velocity direction corresponds to the change of the shape of the flame front. It shows that the direction of the flow is one of the factors that cause the change of the shape of the flame front.

The right column of Figure 12 shows experimental velocity curves at corresponding times. The longitudinal axis represents the length of the tube (x-axis, unit: cm) and the transverse axis represents the flow velocity (unit: m/s). The curves in Figure 12 show the velocity component in the x direction at a height of y = 1 cm at a certain time. The velocity of the flow in the tube is characterized by the x direction velocity component, because the velocity in the

longitudinal direction of the tube is far greater than in the transverse direction for a tube with large length-to-diameter ratio. The change of the flame front shape is more obvious in the direction of the length, which is closely related to the larger velocity component of the *x* direction. At the same time, the flow near the side wall will be affected by the wall surface, and the flow near the centerline (y = 0 cm) will be affected by the flow field in the lower half, so the velocity of the core flow field is characterized by the velocity at height of y = 1 cm.

The velocity graph and vector graph together show the magnitude and direction of the flow field in the tube at the same time. The velocity curves (right column of Figure 12) show that the velocity of gas flow in the first stage increases gradually, the peak velocity appears in front of the flame front, and the velocity of the flow field reaches its maximum (about 6 m/s) in the period of 5 to 10 ms. After 10 ms, although the flow direction is constant, the flow field has entered the deceleration stage. During the period of 20 to 25 ms, the back boundary of the flame front shows a tensile change in the direction of the reverse flame propagation, and gradually forms a "tulip" flame. The reverse velocity of the combustion product is close to the maximum value of about -3 m/s for the first time, which means that the formation of the "tulip" flame can be related to the reverse flow velocity.

In order to further prove the effect of flow velocity on flame propagation, the boundary conditions for Case 15 are changed by setting a pressure outlet at the closed end of the tube, and the flame propagation process is simulated with one closed end and the other an open end. The simulation results are shown in Figure 13. The velocity direction caused by deflagration under the opening condition is consistent with the direction of flame propagation, and the velocity of the flow field in the tube increases continuously, which is more than 25 m/s when the flame reaches the tube mouth, while the maximum velocity under the closed condition is

only about 6 m/s. Besides, there is no "tulip" shape on the flame front, and the "finger" flame form is always maintained. Under this condition, the time from ignition to the flame arriving at the tube outlet is less than 15 ms, but the corresponding experimental results show that flame propagation in the closed tube is more than 45 ms. Judging from the propagation time, the flame speed has been greatly increased under the open-tube condition, and has undergone a remarkable accelerated propagation process. It is thus proved that the change of the tube end condition affects the direction of the flow velocity, which significantly affects the flame propagation velocity and the flame shape.

Through the analysis of the influence of flow velocity on flame propagation, the flow velocity is identified to be one of the main factors determining the flame propagation process. The study of flame acceleration mechanism can be further analyzed from the angle of flow field caused by flame propagation, which provides a new research direction for this problem.

6.2 Turbulence

The turbulent flow caused by flame propagation has become a widespread consensus as a flame acceleration mechanism. Theoretical study suggests that the increase of turbulent combustion velocity is the cause of flame acceleration. However, experiments have also shown that the flow of high turbulence causes excessive stretching of the flame front to cause extinction, and the turbulent combustion velocity does not increase with the increase of turbulence limitlessly (Ciccarelli and Dorofeev 2008). That is to say, the contribution of turbulent combustion velocity to the increase of flame speed is limited, and up to now, it is not clear how much this contribution is. This section applies numerical simulation to carry out a preliminary exploration of this problem.

In the study of flame accelerated propagation, obstacles are usually added in the tube to introduce turbulence, so as to study the effect of turbulence on flame acceleration. In this paper, we use this method by adding obstacles to the geometric model of Case 15.

An obstacle is a bar with rectangular cross-section. The length is equal to 3.8 cm, which is the same as the width of tube (*z* axis), as shown in Figure 14 (a). Seven obstacles are evenly arranged along the length direction of the tube (*x* axis), as shown in Figure 14 (b). The width of the obstacle is 0.6 cm, and according to the difference of the Blockage Ratio (BR), three different heights (h_o) of obstacles are used, that is, BR = 0.3, h_o = 0.57 cm; BR = 0.5, h_o = 0.95 cm; BR = 0.7,h_o = 1.33 cm. The definition of the blocking ratio is as follows:

$$\mathrm{BR} = 1 - \frac{h}{H} \tag{16}$$

where the dimensions of *H* and *h* are shown in Figure 14.

Other settings of numerical simulation are the same as those of Case 15.

The numerical simulation results of the flame propagation process with different blocking ratios are shown in Figure 15. The nephogram of the vertical and horizontal (longitudinal) section on the central axis of the tube represents the change of the flame with the height and length of the tube, while the equivalent surface of the process variable *C* = 0.05 represents the distribution of the flame in space. As shown in the picture, in the process of flame propagation, under the disturbance of the obstacle, the flame front between two adjacent obstacles is strongly stretched and a recirculating zone is formed in the rear of the obstacle. The larger the blocking ratio, the more obvious is the recirculating zone. As the flame propagates, the unburned premixed gas is wrapped by the flame front, and the original

continuous flame front is broken, resulting in an irregular form. The larger the obstruction ratio, the more significant is the effect of obstacles on flame propagation, and the degree of irregularity of flame front is more pronounced at the same time.

By comparing the propagation distance of the flame array front under different blocking ratios at the same time, it can be seen that the greater the blocking ratio, the faster is the flame spread in the direction of the tube.

The development of turbulence is represented by the dimensionless value of the root-mean-square of the turbulent fluctuating velocity (from 1 ms to 15 ms) on the central axis of the tube, as shown in Figure 16. With the propagation of flame, the turbulence intensity of flow field in the tube increases first and then decreases. The initial stage of flame propagation is an acceleration process, and the turbulence intensity increases gradually under the action of flame and obstacles. After that, the flame is affected by the closed end and enters the stage of deceleration. The velocity in the tube decreases and the turbulence decreases. The larger the blocking ratio, the larger is the velocity and amplitude of turbulence.

Previous analysis shows that the presence of obstacles would increase the turbulence of the flow field in the tube. The greater the blockage ratio, the greater is the turbulence intensity. The velocity distribution in the *x* direction (central axis) of the tube at different times is plotted in Figure 17. From the figure, it can be seen that at the same time, when the flame front and the premixed gas in front of the flame front pass between the upper and lower obstacles in a pair, the flow speeds up, and the velocity decreases after the obstacles. The larger the blocking ratio, the more obvious is this phenomenon. For the three selected moments, the maximum value of the *x* component of velocity always lags behind the flame

front, and the distance between them increases with flame propagation. Compared to the results of the Case 15 without obstacle, where the flame front is basically synchronized with the peak velocity, it is believed that the enhancement of the turbulence intensity by the obstacle may form a strong tension on the flame front, which makes the front of the flame easily bypass the obstacles. The premixed gas between the adjacent obstacles is not fully burned when the front of the flame passes through. Thus after that, the thermal expansion of this part of the premixed gas begins to appear. That is why the velocity peak is formed after the flame front. If the flow generated by the delayed thermal expansion is regarded as a "jet", the lagging jet not only can increase the turbulence of the flow field, but also promote the spread of the advanced flame, which may be a possible mechanism of flame acceleration caused by obstacles.

As mentioned above, turbulent combustion velocity is one of the causes of flame acceleration, and its contribution to the increase of flame speed is limited. The dimensionless turbulent combustion velocity (S_T) and flame propagation velocity (S_F) are plotted in Figure 18, under the same blocking ratio, where S_L is laminar burning velocity. As shown in Figure 18, S_T gradually increases during the flame propagation, and the variation of S_T corresponds to the degree of turbulence. Compared with the increase of S_T in different blockage ratio conditions, it can be seen that, although the turbulence intensity varies greatly under different blocking ratios, the maximum value of S_T corresponding to different turbulence intensity is very similar. The dimensionless turbulent combustion velocity lies between 10 and 15, which indicates that there is a limit to the increase of S_T due to turbulence, and S_T is not always proportional to the change of turbulence. In the process of increasing turbulence, the flame propagation velocity S_F is always greater than S_T, and when the increase of S_T is very

small, S_F is still increasing. Thus, it can be seen that S_T can only be one of the factors affecting S_F. Moreover, when the flow development reaches a certain degree of turbulence, the degree of influence of S_T on S_F is gradually weakened. Instead, some other factors have contributed to the continuous increase of S_F. It is worth noting that these factors always exist, and will become the main reason for the acceleration of the flame with the development of the flow. If these factors are generalized into the characteristics of the flow field, the flame velocity can be expressed as a piecewise function

$$\text{Flame velocity} = \begin{cases} f\left(S_{\mathrm{T}},\ \text{Flow field characteristics}\right) & S_{\mathrm{T}} < \beta S_{\mathrm{L}} \\ f\left(\text{Flow field characteristics}\right) & S_{\mathrm{T}} > \beta S_{\mathrm{L}} \end{cases} \tag{17}$$

In formula (17), β is the maximum of ratio of turbulent combustion velocity to laminar burning velocity. Based on the numerical simulation results in this section, $\beta \approx 15$; but the maximum turbulent combustion velocity observed experimentally is about 10 times the laminar burning velocity (Ciccarelli and Dorofeev 2008) and $\beta \approx 10$. No matter what value of β is used, as the flame accelerates, the turbulent combustion velocity will be close to a fixed value. Then the mechanism of flame acceleration is completely related to the characteristics of the flow field, and the influence of the turbulent combustion velocity can be neglected to simplify the study of the problem.

Therefore, the acceleration mechanism of turbulence to flame propagation varies periodically. The low-intensity turbulence increases the area of the flame front through wrinkling, bending and stretching. This increases the combustion reaction rate, transforms the laminar combustion velocity into a turbulent combustion velocity including the action factors of the flow field, and changes the heat and mass transport mechanism of the chemical reaction

gradually from the diffusion to the vortex mass transport. Thus, the combustion process is essentially influenced by turbulence and the turbulent combustion velocity is increased to the limit. The effect of turbulence on flame acceleration is manifested in two aspects, namely, combustion and characteristics of flow field. The high-intensity turbulence does not significantly change the chemical reaction process, but changes the characteristics of the flow field and influences the shape of the flame front, making flame dispersed or broken, and the flame accelerating propagation is controlled by the change of the flow field itself.

7. Conclusions

Large eddy simulation (LES) was used to study the flame propagation of methane-air premixed gas in square tubes of different lengths. Compared with the experimental results of flame propagation distance, flame velocity and flame pressure, the simulated results can accurately describe the flame propagation characteristics. The LES method and the premixed flame model can be used to demonstrate or predict real flame propagation process, which can be used for further analysis of deflagration flame propagation.

The cause of “tulip” flame was studied in the accessible tube. The analysis of the flow field on flame propagation indicates that the flow velocity is one of the main factors that determine flame shape and affect the flame propagation process. The reverse flow velocity on the combustion product side is the cause of flame deceleration. The change of the flow direction and the velocity difference in front of and behind the flame front may be one of the causes in the formation of “tulip” flame.

In order to study the effect of turbulence on flame acceleration, obstacles were added to the

tube to make the flow field turbulent. The mechanism of the effect of turbulence on flame acceleration changes periodically. In the initial stage of propagation, turbulent flow increases the surface area of flame by means of folding, bending and stretching, and makes the laminar burning transit to turbulent combustion together with the action factors of the flow field. In this stage, flame acceleration is affected by both turbulent combustion and other flow field characteristics. With the continuous development of turbulence, the turbulent combustion speed increases and reaches a limit and becomes stable. Turbulent combustion no longer affects flame acceleration, and only flow field characteristics are the control factors. The effect mechanism of turbulent on flame propagation can be expressed in a piecewise functional form

$$\text{Flame velocity} = \begin{cases} f\left(S_{\mathrm{T}},\ \text{Flow field characteristics}\right) & S_{\mathrm{T}} < \beta S_{\mathrm{L}} \\ f\left(\text{Flow field characteristics}\right) & S_{\mathrm{T}} > \beta S_{\mathrm{L}} \end{cases}$$

where β is the maximum of ratio of turbulent combustion velocity to laminar burning velocity, $10 < \beta < 15$.

Appendix A: Flow Equations

Mass conservation equation

$$\frac{\partial \rho}{\partial t} + \frac{\partial \left(\rho u_i\right)}{\partial x_i} = 0 \tag{A1}$$

Momentum conservation equation

$$\frac{\partial(\rho u_j)}{\partial t}+\frac{\partial(\rho u_i u_j)}{\partial x_i}=-\frac{\partial p}{\partial x_j}+\frac{\partial \tau_{ij}}{\partial x_i}+F_j \qquad \text{(A2)}$$

Energy conservation equation

$$\frac{\partial(\rho h)}{\partial t}+\frac{\partial(\rho u_i h)}{\partial x_i}=\frac{\partial p}{\partial t}-\frac{\partial Q_i}{\partial x_i}-\frac{\partial(u_i \tau_{ij})}{\partial x_j}+S_r \qquad \text{(A3)}$$

Calculation of density ρ (kg/m^3) by using ideal gas equation of state as:

$$\rho = p \Big/ \left(RT \sum_{\alpha=1}^{N} \frac{Y_\alpha}{M_\alpha} \right) \qquad \text{(A4)}$$

In the above equation, p is pressure in Pa; T is temperature in K; N is the number of substances (methane and air in this work, $N = 2$); Y_α is the mass fraction of component α, α = 1, 2; and M_α is the molecular weight of component α in kg/mol.

In equation (A2), F_j is volume force in N; the gravity effect is neglected, $F_j = 0$; and τ_{ij} is the viscous stress tensor.

$$\tau_{ij} = \mu s_{ij} - \frac{2}{3}\mu \frac{\partial u_k}{\partial x_k}\delta_{ij} \qquad \text{(A5)}$$

with

$$s_{ij} = \frac{\partial u_i}{\partial x_j} + \frac{\partial u_j}{\partial x_i} \tag{A6}$$

In equation (A5), μ is the dynamic viscosity coefficient in N·s/m^2; and δ_{ij} is the unit tensor.

In equation (A3),

$$h = \frac{1}{2} u_i u_j + \sum_{\alpha=1}^{N} Y_\alpha h_\alpha \tag{A7}$$

$$h_\alpha = H_\alpha + \int_{T_{ref}}^{T} c_{p,\alpha} \mathrm{d}T \tag{A8}$$

$$Q_j = -\kappa\rho \frac{\partial h}{\partial x_j} \tag{A9}$$

h is enthalpy in J; and S_r is radiation heat loss in W. In this paper, the loss of radiation heat is ignored, that is $S_r = 0$; H_α is heat generated by component α in J; Q_j is heat flux density in W/m^2; and κ is thermal conductivity in W/(m·K).

Besides, the premixed combustion model simulates the chemical reaction process of converting premixed gas to combustion product through process variable *C* defined by:

$$C = \frac{\sum_{\alpha=1}^{n} Y_{\alpha}}{\sum_{\alpha=1}^{n} Y_{\alpha,\mathrm{eq}}} \tag{A10}$$

In the above equation, Y_{α} is the mass fraction of the combustion product α; $Y_{\alpha,\mathrm{eq}}$ is the final mass fraction of the combustion product α. In this work, the combustion products of methane-air premixed gases are two kinds, carbon dioxide and water, respectively. From the definition of the process variable *C*, it can be seen that *C* can represent the change of the mass fraction of the combustion product, so for the premixed gas, $C = 0$, and for the combustion product, $C = 1$.

Using the transport equation of *C*, the process of the chemical reaction in the turbulent flow is described in time and space. In fact, the gradient of *C* represents the flame front.

The transport equation of the density weighted average of $\overline{C}$ to be solved in FLUENT is:

$$\frac{\partial\left(\rho\overline{C}\right)}{\partial t} + \frac{\partial\left(\rho u_i \overline{C}\right)}{\partial x_i} = \frac{\partial}{\partial x_i}\left(\rho D_{\mathrm{L}} \frac{\partial \overline{C}}{\partial x_i}\right) + \rho S_{\mathrm{r}} \tag{A11}$$

In the above equation, $\overline{C}$ is the density-weighted mean of *C*; D_L (in m^2/s) is the mass diffusion coefficient; S_r (in s^{-1}) is the chemical reaction process source term; and ρS_{r} is the average rate of chemical reaction, calculated in terms of premixed gas density ρ_{u} (in kg/m^3) and turbulent combustion speed S_{T} (in m/s):

$$\rho S_r = \rho_u S_T |\nabla C| \quad \text{(A12)}$$

The key to describe flame propagation in the premixed flame model is to solve the transport equation of *C*. That is, the solution of the rate term of the chemical reaction (ρS_r), and the simulation of (ρS_r) depends on the calculation of the turbulent combustion velocity. For the *C*-equation model, the Zimont model is selected to describe the turbulent combustion velocity.

The Zimont turbulent combustion velocity model is established based on two factors, the laminar combustion velocity and the influence of the large eddy and the small eddy on the wrinkle stretching and thickening of the flame front. At the same time, the effect of turbulence on flame stretching and the influence of premixed gas mass diffusivity on heat release intensity are also considered. Its mathematical expression is not the focus of this study, and it is limited by space and not described in detail here.

Declaration

The authors declare that they have no conflict of interest.

References

Blanchard R, Arndt D, Gratz R, Scheider S (2011). Effect of ignition position on the run-up distance to DDT for hydrogen-air explosions. *Journal of Loss Prevention in the Process Industries*, 24(2): 194-199.

Charlette F, Meneveau C, Veynante D (2002). A power-law flame wrinkling model for LES

of premixed turbulent combustion. Part I. Non-dynamic formulation and initial tests. *Combustion and Flame*, 131(1-2): 159-180.

Chow WK (2014). A study on explosion hazards of clean refrigerant propane leaking from air-conditioning units in small commercial flats. GRF project funded by the Research Grants Council of Hong Kong.

Chow WK, Pang ECL (2012). Fire safety of adjacent areas to oil tanks and fire protection systems proposed. Poster presented at the 2nd Asian-US-European Thermophysics Conference-Thermal Science for Sustainable World, 3-6 January 2012, Hong Kong.

Ciccarelli G, Dorofeev S (2008). Flame acceleration and transition to detonation in ducts. *Progress in Energy and Combustion Science*, 34(4): 499-550.

Di Sarli V, Di Benedetto A, Russo G (2010). Sub-grid scale combustion models for large eddy simulation of unsteady premixed flame propagation around obstacles. *Journal of Hazardous Materials*, 180(1-3): 71-78.

Dunn-Rankin D, Sawyer RF (1998). Tulip flames: changes in shape of premixed flames propagating in closed tubes. *Experiments in Fluids*, 24(2): 130-140.

Ellis OC, Wheeler RV (1928). Explosion in closed cylinders. Part III. The manner of movement of flame. *Journal of Chemical Society*, Part 2: 3215-3218.

Fiorina B, Vicquelin R, Auzillon P, Darabiha N, Gicquel O, Veynante D (2010). A filtered tabulated chemistry model for LES of premixed combustion. *Combustion and Flame*, 2010, 157(3): 465-475.

Fureby C (2005). A fractal flame-wrinkling large eddy simulation model for premixed turbulent combustion. *Proceedings of the Combustion Institute*, 30(1): 593-601.

Gubba SR, Ibrahim SS, Malalasekera W, Masri AR (2011). Measurements and LES calculations of turbulent premixed flame propagation past repeated obstacles. *Combustion and Flame*, 158(12): 2465-2481.

Hermanns RTE, Konnov AA, Bastiaanseta RJM, de Goey LPH, Lucka K, Köhne H (2010). Effects of temperature and composition on the laminar burning velocity of CH_4+H_2+O_2+N_2 flames. *Fuel*, 89(1): 114-121.

Huo Y, Chow WK (2017). Flame propagation of premixed liquefied petroleum gas explosion in a tube. *Applied Thermal Engineering*, 113: 891-901.

Jenkins CM, Ripley RC, Wu CY, Horie Y, Powers K, Wilson WH (2013). Explosively driven particle fields imaged using a high speed framing camera and particle image velocimetry. *International Journal of Multiphase Flow*, 51(5):73-86.

Knudsen E, Pitsch H (2008). A dynamic model for the turbulent burning velocity for large eddy simulation of premixed combustion. *Combustion and Flame*, 154(4): 740-760.

Liberman MA, Kuznetsov M, Ivanov A (2009). Formation of the preheated zone ahead of a propagating flame and the mechanism underlying the deflagration-to-detonation transition. *Physics Letters A*, 373: 501-510.

Moureau V, Fiorina B, Pitsch H (2009). A level set formulation for premixed combustion LES considering the turbulent flame structure. *Combustion and Flame*, 156(4): 801-812.

Ng YW, Chow WK (2015). Use of clean refrigerant and their potential fire hazards in Hong Kong. ASME-ATI-UIT 2015 Conference on Thermal Energy Systems: Production, Storage, Utilization and the Environment, 17-20 May 2015, Napoli, Italy.

Ng YW, Huo Y, Chow WK, Chow CL, Cheng FM (2017). Numerical simulations on explosion of leaked liquefied petroleum gas in a garage. *Building Simulation - An International Journal*, 10 (5): 755-768.

Orana ES, Gamezo VN (2017). Towards scaling laws for DDT in obstructed channels. Topical Review, Paper presented at Eighth International Symposium on Scale Modeling (ISSM-8), Portland, Oregon, USA, 12-14 September 2017.

Porowski R, Teodorczyk A (2013). Experimental study on DDT for hydrogen-methane-air

mixtures in tube with obstacles. *Journal of Loss Prevention in the Process Industries*, 26(2): 374-379.

Rigby SE, Fay SD, Tyas A, Warren JA, Clarke SD (2015). Angle of Incidence Effects on Far-Field Positive and Negative Phase Blast Parameters. *International Journal of Protective Structures*, 6(1): 23-42.

Salamandra GD, Bazhenova TV, Naboko IM (1959). Formation of detonation wave during combustion of gas in combustion tube. *Proceedings of the Combustion Institute*, 7: 851-855.

Silvestrini M, Genova B, Parisi G, Trujillo FJL (2008). Flame acceleration and DDT run-up distance for smooth and obstacles filled tubes. *Journal of Loss Prevention in the Process Industries*, 2008, 21: 555-562.

Teodorczyk A, Drobniak P, Dabkowski A (2009). Fast turbulent deflagration and DDT of hydrogen-air mixtures in small obstructed channel. *International Journal of Hydrogen Energy*, 34(14): 5887-5893.

Thomas G, Oakley G, Bambrey R (2010). An experimental study of flame acceleration and deflagration to detonation transition in representative process piping. *Process Safety and Environmental Protection*, 88: 75-90.

Table 1 Numerical simulation conditions in the literature (Dunn-Rankin and Sawyer 1998)

Example case		Case 6	Case 15
Computing domain		3.8 cm by 3.8 cm by 6 cm long	3.8 cm by 3.8 cm by 15 cm long
Grid partition	Grid type	Structured grid	
	Grid size	Minimum grid 1.1e-10 m^3 Maximum grid 4.1e-10 m^3	Minimum grid 1.36e-10 m^3 Maximum grid 5.1e-10 m^3
	Grid number	86436	174636
Time step (s)		5×10^{-7}	1×10^{-7}
Initial condition		300 K 1.01325e+05 Pa Process variable C = 0	
Model setting	Turbulence model	Large Eddy Simulation	
	Subgrid model	Dynamic Smagorinsky-Lilly Model	
	Combustion model	Premixed Combustion Model	
	Turbulent combustion velocity model	Zimont Turbulent Flame Speed Model	
Premixed gas attribute	Density calculation	Ideal Gas Model	
	Specific heat capacity, J/(kg·K)	1123.795	
	Thermal conductivity, W/(m·K)	0.0244	
	Viscous, kg/(m·s)	1.73845e-05	
	Laminar combustion speed, m/s	0.365 (Hermanns et al. 2010)	
	Mass fraction of combustibles	0.055	

Figure Captions

Fig. 1 Physical model of flame propagation
Fig. 2 Z-type Schlieren photography system
Fig. 3 Computational domain of flame propagation simulation in a tube without obstacles
Fig. 4 Contours of progress variable for flame propagation of Case 6
Fig. 5 Contours of process variable for flame propagation of Case 15
Fig. 6 Flame front position for Case 6. Upper part: experimental, lower part: simulation
Fig. 7 Flame front position for Case 15. Upper part: experimental, lower part: simulation
Fig. 8 Comparison of flame front position
Fig. 9 Average value of flame speed
Fig. 10 Comparison of simulated flame speeds with experimental values
Fig. 11 Comparison of absolute pressure in the tube
Fig. 12 Flow field and flame propagation in the 15-cm long tube. The transverse axis represents the axial position and the longitudinal axis represents the height of the tube, in centimeters
Fig. 13 Flow direction induced by flame propagation in the 15-cm tube with vent
Fig. 14 Obstacles set up in the tube
Fig. 15 Flame propagation in the tube with different obstacle blockage ratios
Fig. 16 Turbulence states in the tube with different obstacle blockage ratios
Fig. 17 Flow velocity in in the tube with different obstacle blockage ratios
Fig. 18 Contrast of flame speed and turbulence burning velocity

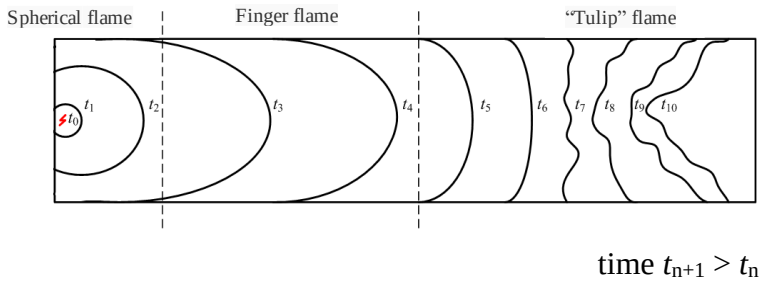

Fig. 1 Physical model of flame propagation

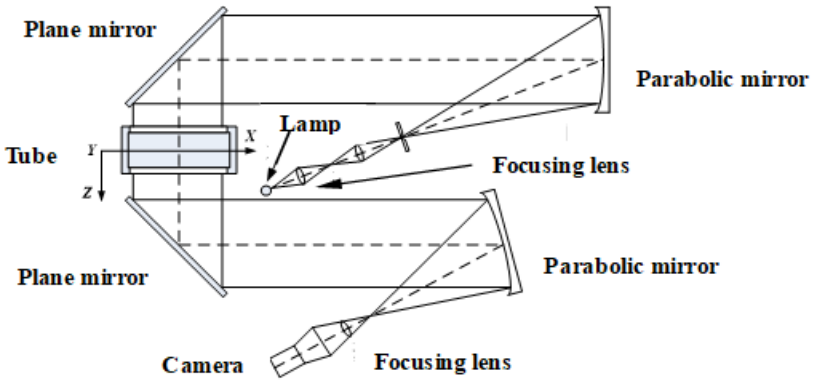

Fig. 2 Z-type Schlieren photography system

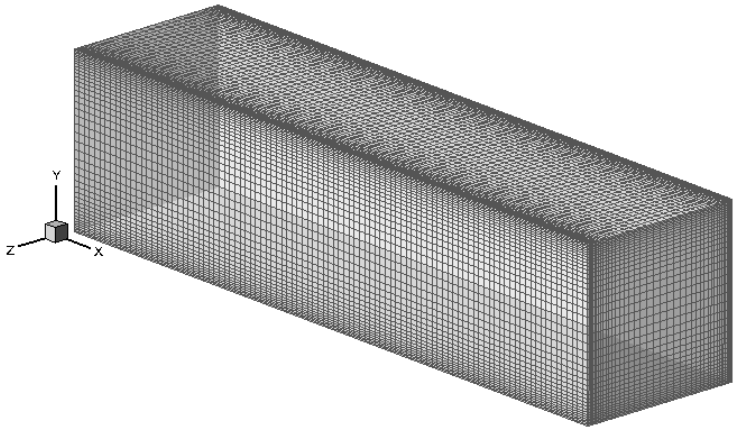

Fig. 3 Computational domain of flame propagation simulation in a tube without obstacles

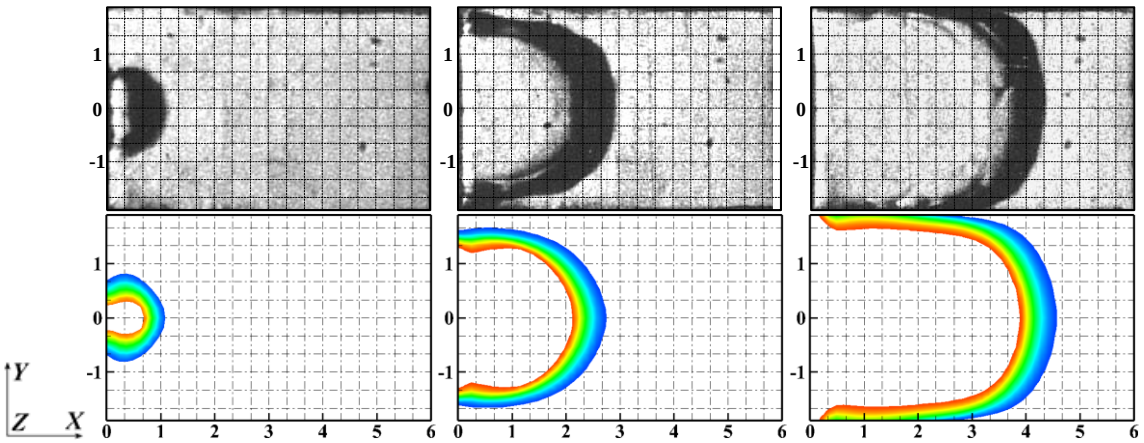

(a) 2.5 ms (b) 7.5 ms (c) 12.5 ms

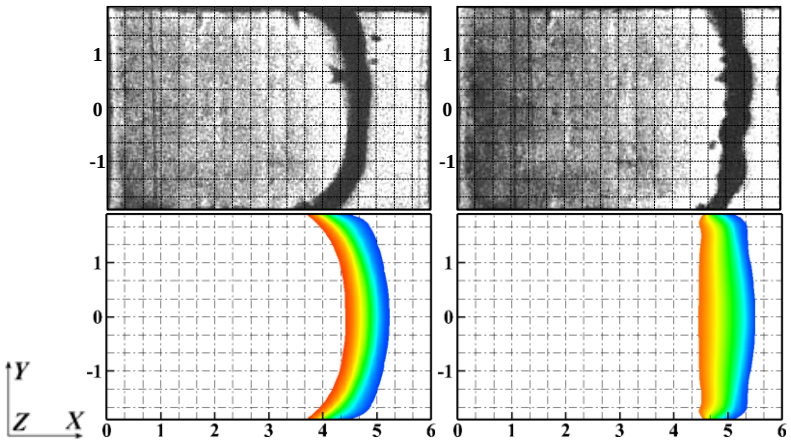

(d) 17.5 ms (e) 22.5 ms

Process variables C:

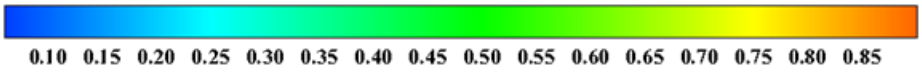

Fig. 4 Contours of progress variable for flame propagation of Case 6

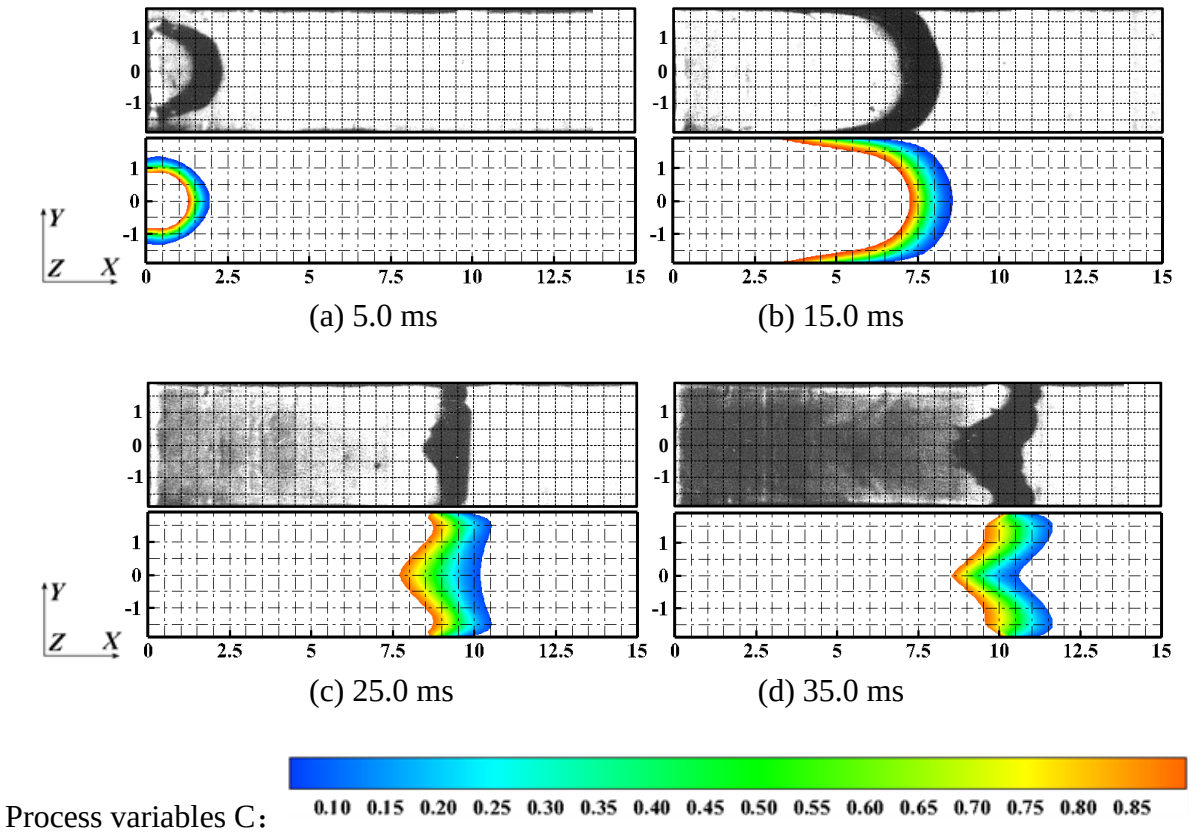

Fig. 5 Contours of process variable for flame propagation of Case 15

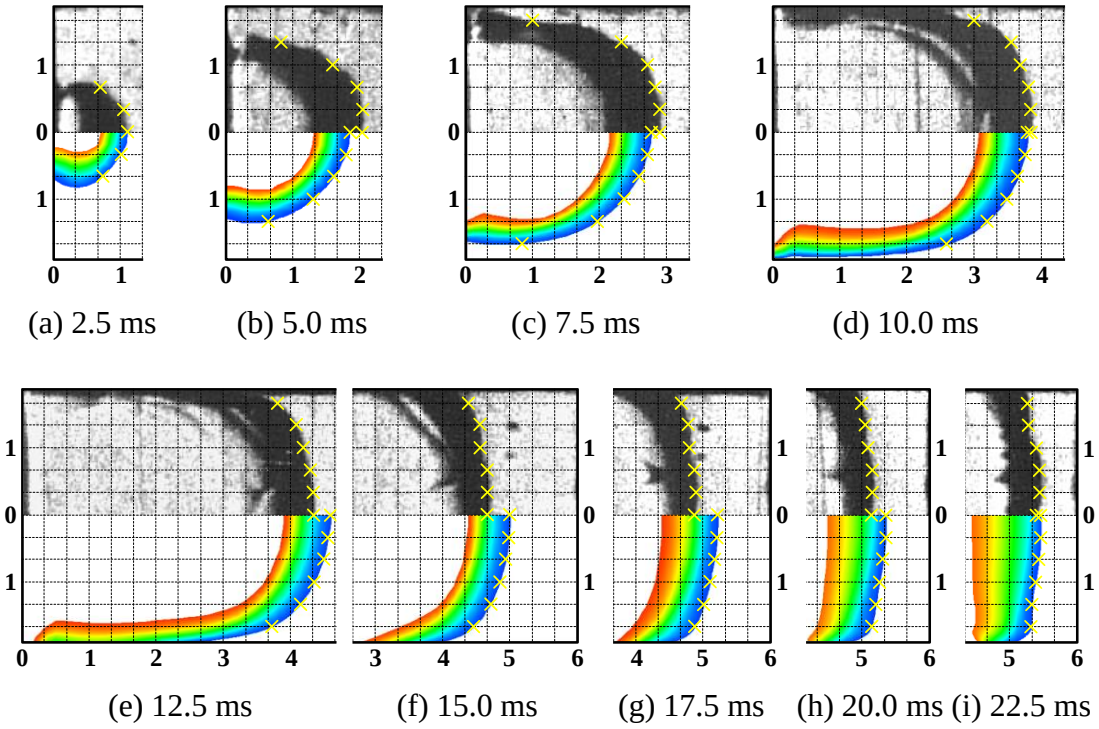

Fig. 6 Flame front position for Case 6. Upper part: experimental, lower part: simulation

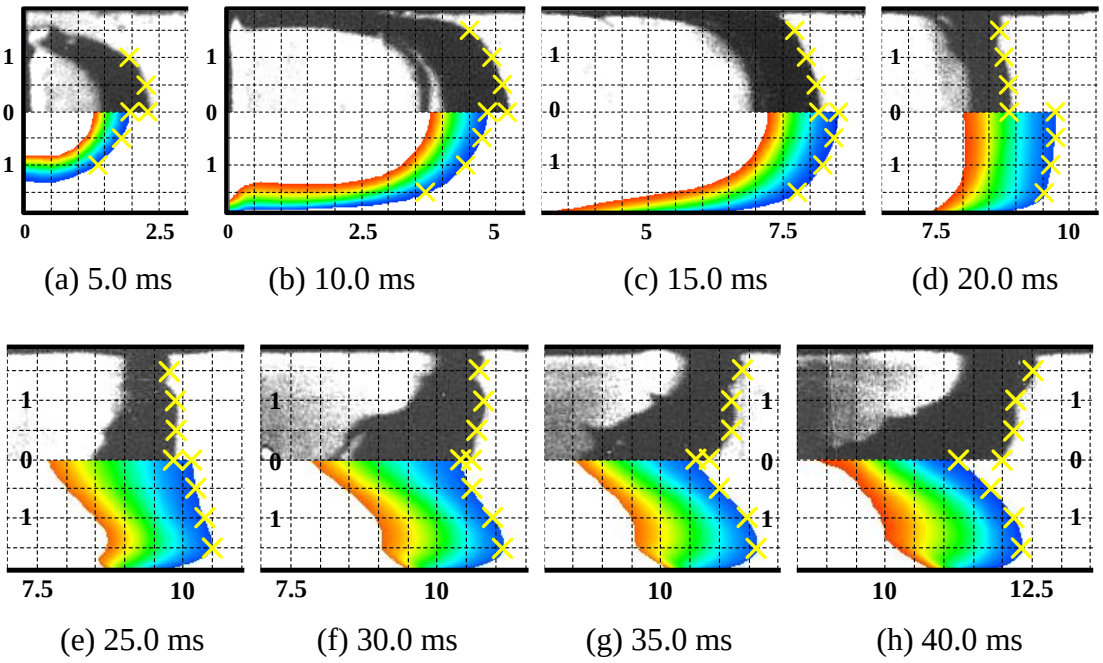

Fig. 7 Flame front position for Case 15. Upper part: experimental, lower part: simulation

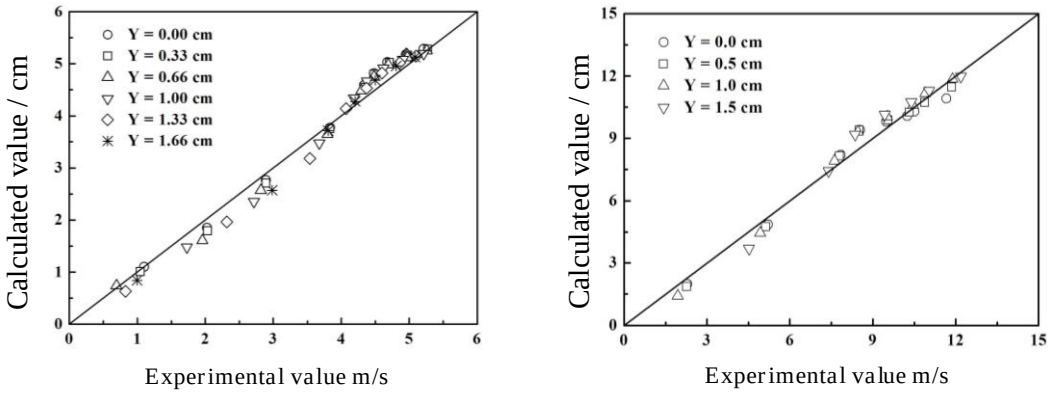

(a) Case 6 (b) Case 15

Fig. 8 Comparison of flame front position

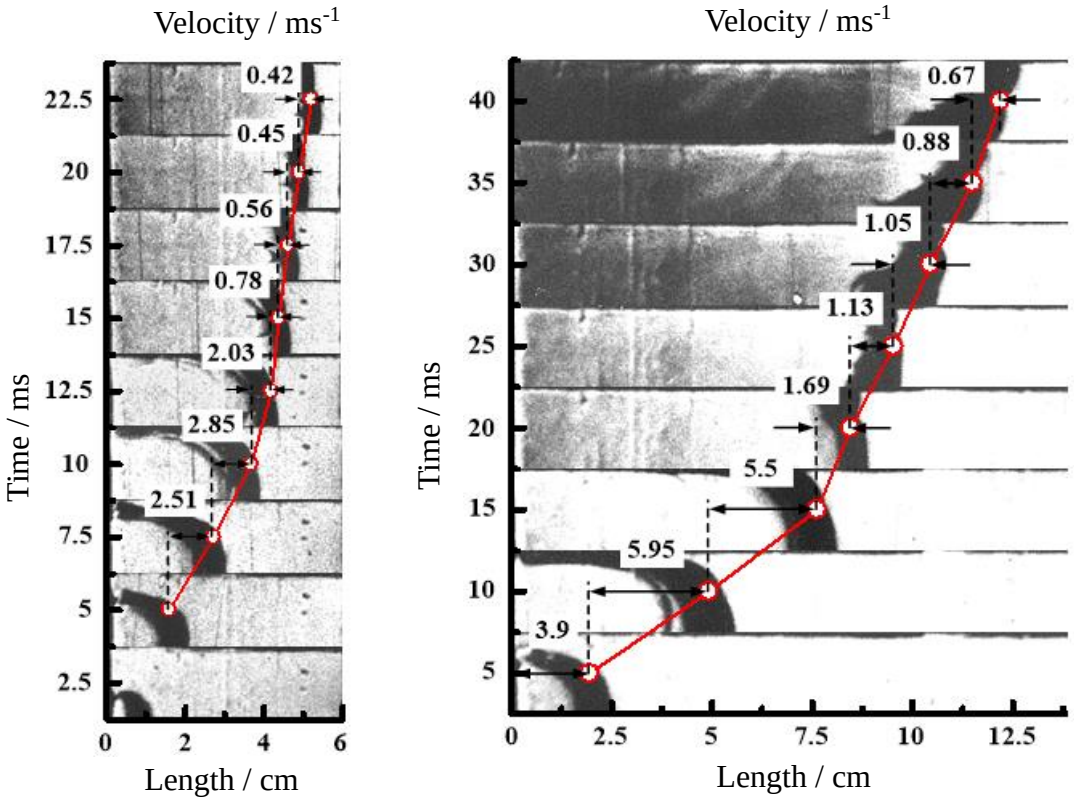

(a) Case 6 (b) Case 15

Fig. 9 Average value of flame speed

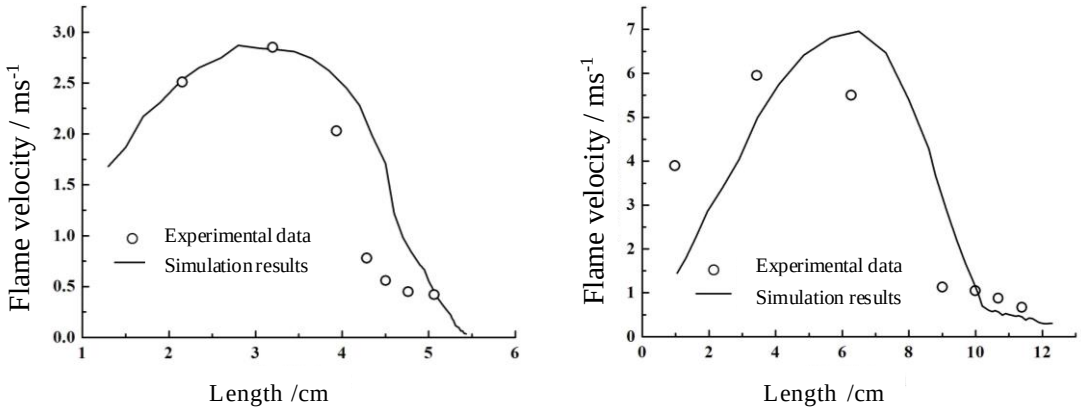

(a) Variation of flame velocity in Case 6 (b) Variation of flame velocity in Case 15

Fig. 10 Comparison of simulated flame speeds with experimental values

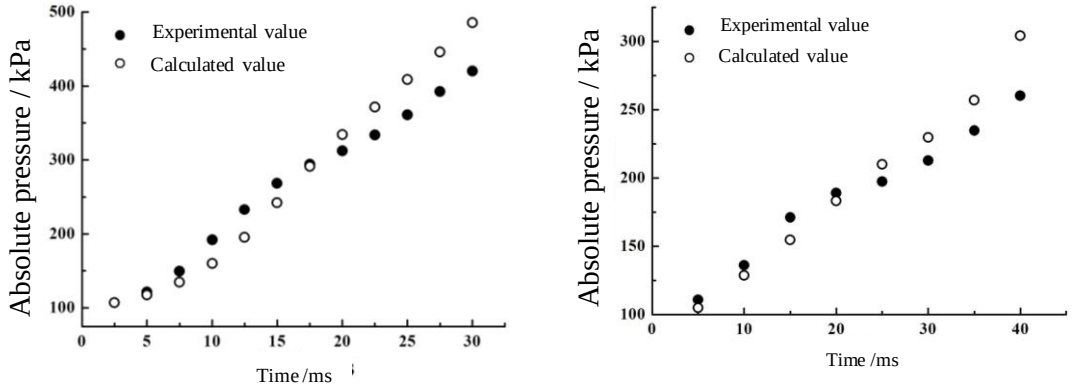

(a) Variation of pressure in Case 6 (b) Variation of pressure in Case 15

Fig. 11 Comparison of absolute pressure in the tube

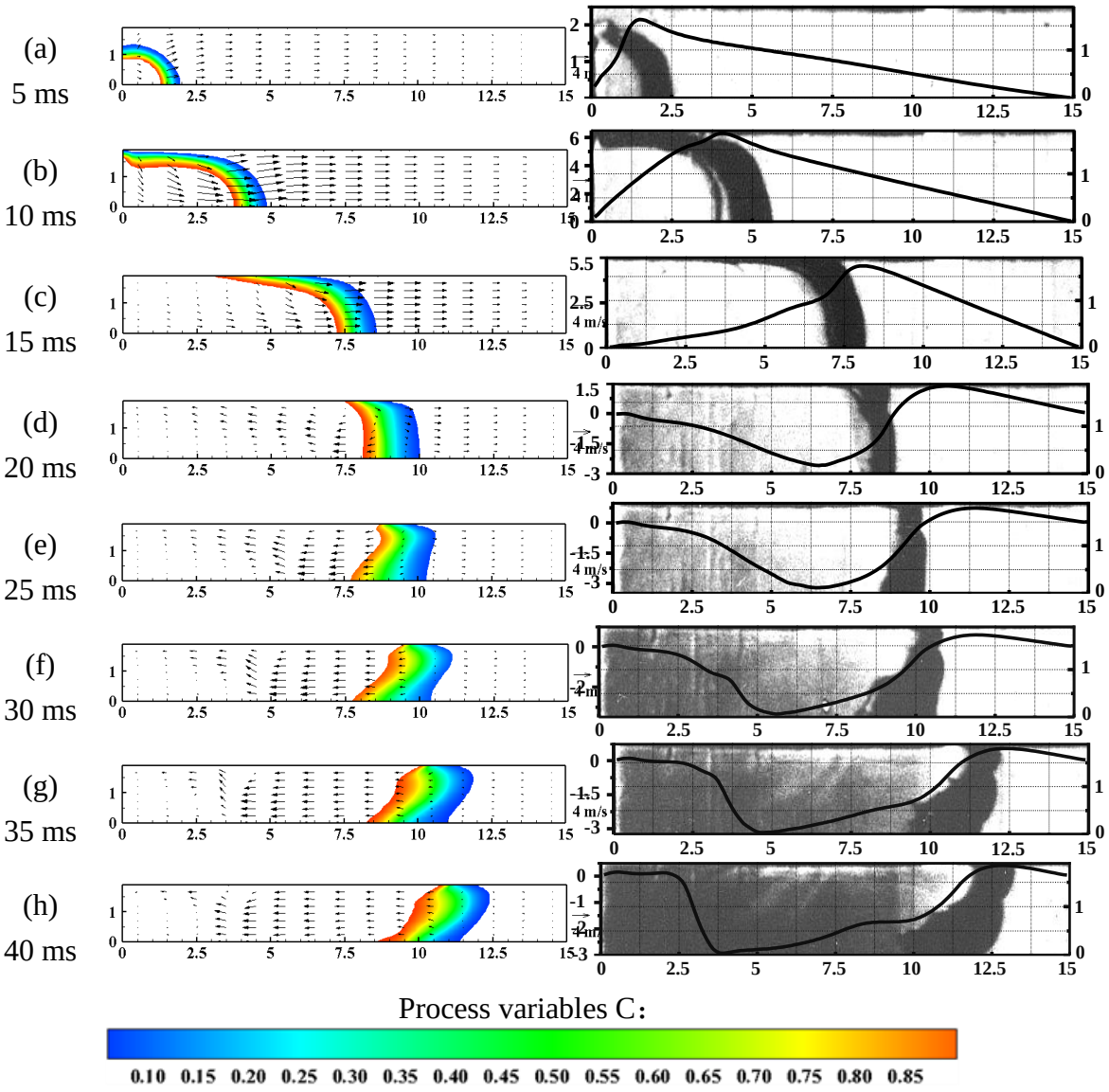

Fig. 12 Flow field and flame propagation in the 15-cm long tube.
The transverse axis represents the axial position and the longitudinal axis represents the height of the tube, in centimeters.

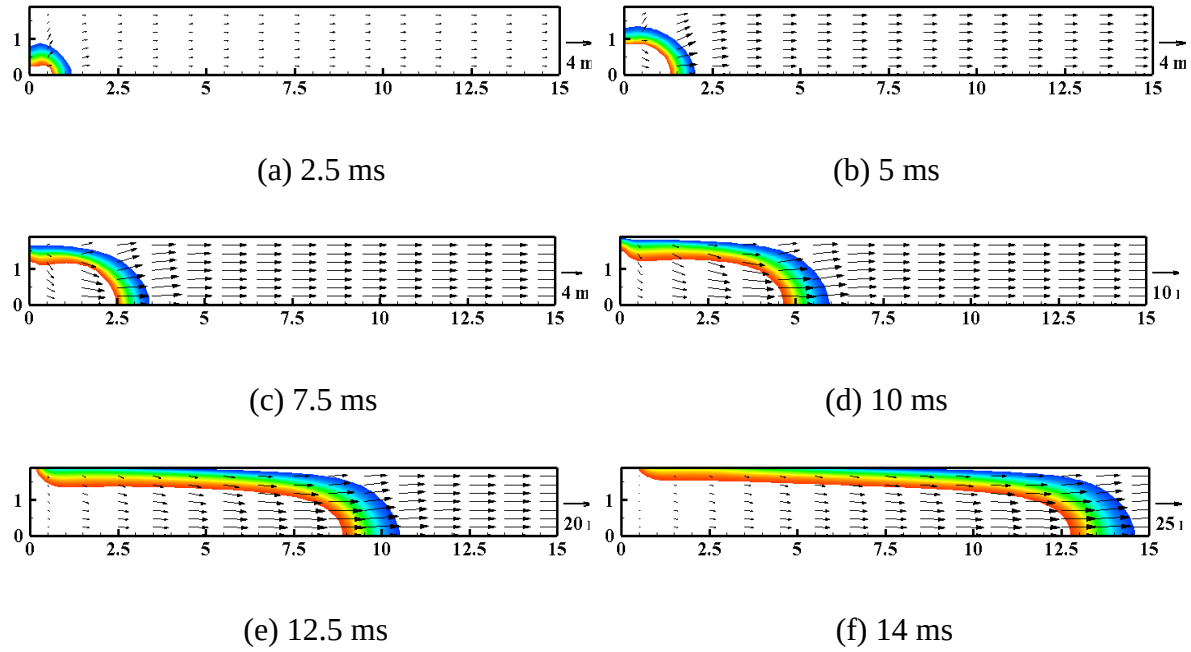

(a) 2.5 ms (b) 5 ms

(c) 7.5 ms (d) 10 ms

(e) 12.5 ms (f) 14 ms

Fig. 13 Flow direction induced by flame propagation in the 15-cm tube with vent

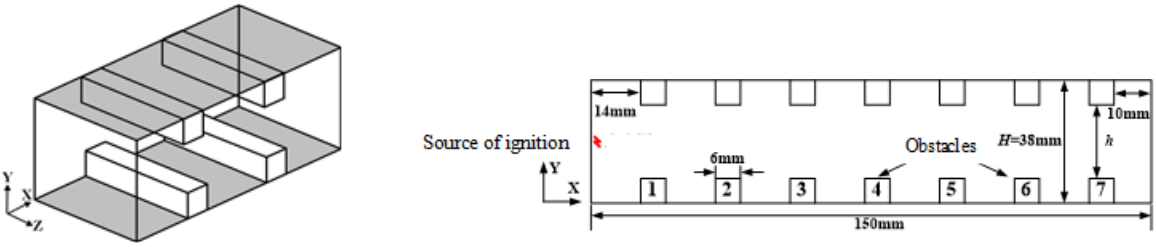

(a) Obstacle form (b) Obstacle position

Fig. 14 Obstacles setup in the tube

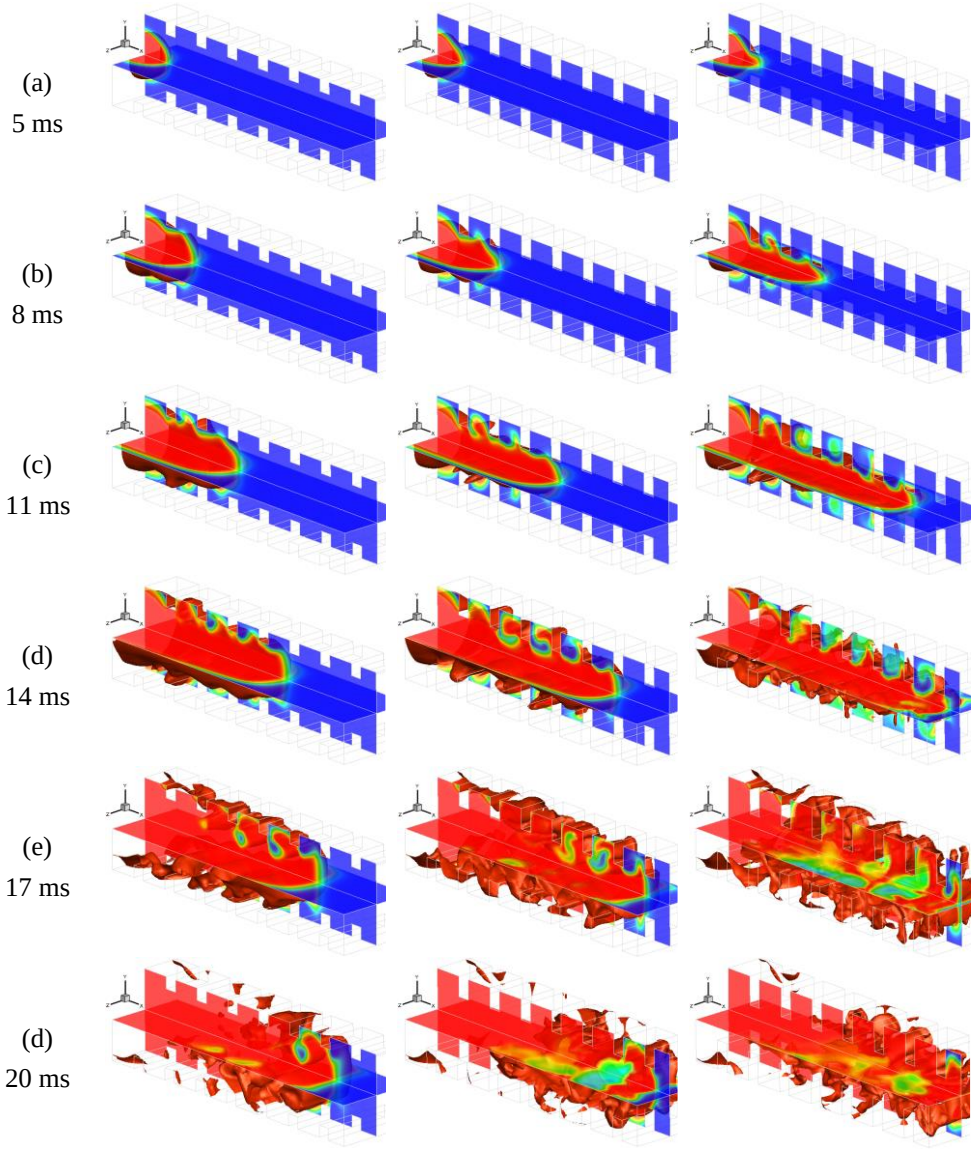

Fig. 15 Flame propagation in the tube with different obstacle blockage ratios

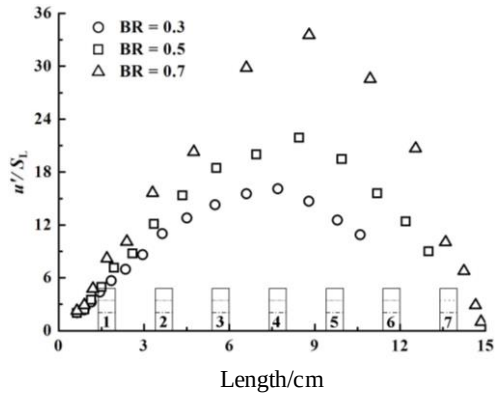

Fig. 16 Turbulence states in the tube with different obstacle blockage ratios

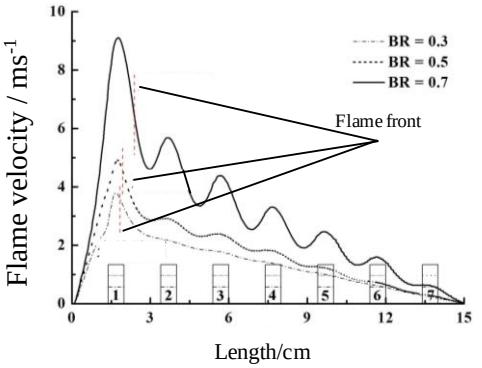

(a) 5 ms

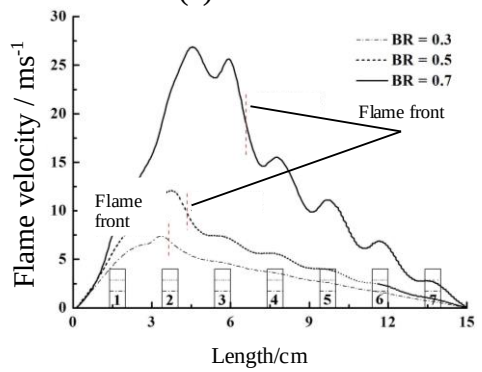

(b) 8 ms

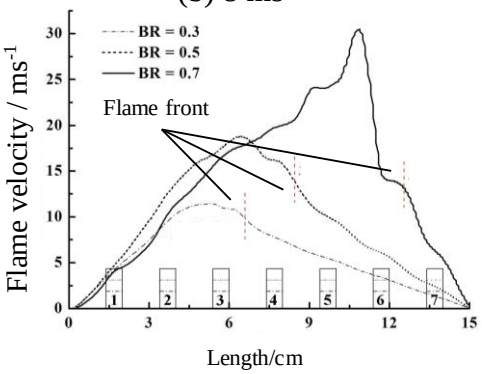

(c) 11 ms

Fig. 17 Flow velocity in the tube with different obstacle blockage ratios

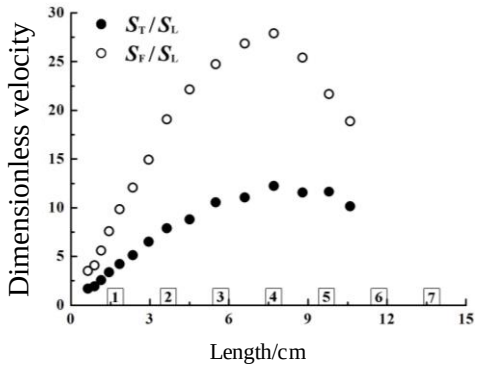

(a) BR = 0.3

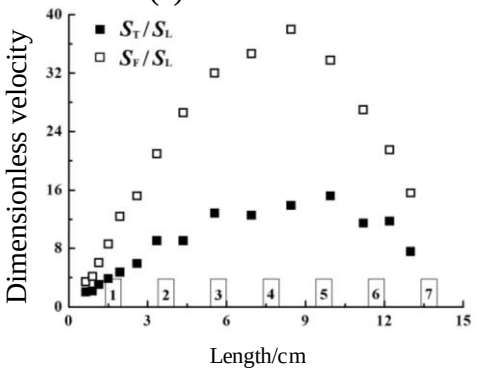

(b) BR = 0.5

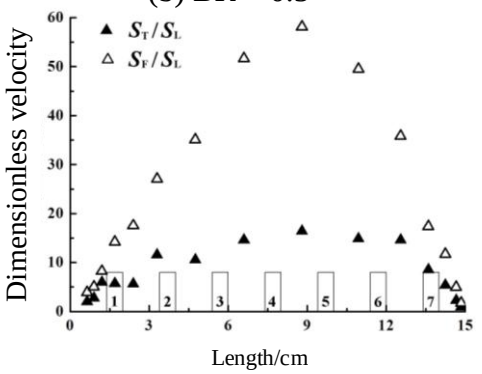

(c) BR = 0.7

Fig. 18 Contrast of flame speed and turbulence burning velocity